Model Reduction using Singular Perturbation Methods for a Microgrid Application

Lasse Gnärig[1], Albrecht Gensior[2], Saioa Burutxaga Laza[3], Miguel Carrasco[4]
Carsten Reincke-Collon[5]
[1]Technische Universität Dresden, Germany, [2]Technische Universität Ilmenau, Germany,
[3]RWE Battery Solutions GmbH, Germany, [4]eMIS Deutschland GmbH, Germany
[5]Aggreko Deutschland GmbH, Germany
[1]lasse.gnaerig@tu-dresden.de, [2]albrecht.gensior@tu-ilmenau.de,
[3]saioa.burutxaga@rwe.com, [4]m.carrasco@emis-deutschland.com,
[5]carsten.reincke-collon@aggreko.com

Keywords

Abstract

The paper deals with the modeling of an island grid for the purpose of simulation. Since the behavior of the system is affected by phenomena taking influence in different time-scales, a model reduction scheme is proposed that leads to simpler models which reduce the computational burden in simulations. Compromises in the modeling procedure are addressed by investigating simulation studies.

Introduction

In contrast to conventional power systems, microgrids mainly fed by inverters have a comparably low physical inertia. This is why studies of stability analysis are of great interest. However, simulating the behavior of such grids may become challenging because the state dimension of the model grows quickly with the size of the network. Furthermore, since such models represent multiple processes associated with different time scales, the step size of the solver is limited by the fast phenomena. Both of these properties increase the computational effort for a simulation of the system [1–5]. In order to overcome this problem, reduced order models can be introduced. The approach proposed here uses singular perturbation theory as an appropriate tool for models with multiple time scales to obtain reduced models of lower order. By applying such methods, a subsystem associated with a short time scale is identified and decoupled from the residual system that evolves on a larger time scale [6–9]. By choosing different sets of variables considered to describe the fast dynamics, multiple models of descending order can be obtained. For the investigation of certain phenomena it is then possible to pick an appropriate model from this set of models [1].

A systematic model reduction procedure for large-signal microgrid models was presented in [1] and also applied in [2–4]. When applying singular perturbation methods, determining the states associated with a short time scale is a non-trivial task. In [2] and [3] this was done by examining the eigenvalues of the state matrix of the linearized microgrid model, whereas in [1] and [4] perturbation parameters were evaluated.

This paper provides a detailed dynamic model of a small microgrid consisting of two grid-forming inverters feeding a passive load. Furthermore, an optional connection to a stiff main grid is considered. The structure of the full order model is adopted from [10]. In order to obtain a detailed model, in contrast to [1], the dynamics of the transmission network and the load are taken into account. A model reduction procedure is introduced which does not require linearization nor the calculation of eigenvalues. Instead, the perturbation parameters are used, derived from the normalized model equations. Normalization ensures that
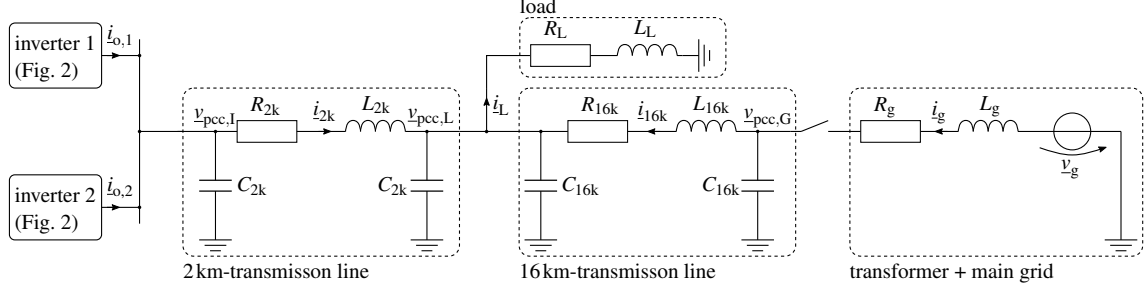
Fig. 1: Configuration of the grid application under investigation. All currents and voltages refer to the common reference frame DQ set by inverter 1.

the magnitudes of the state variables, which can defer greatly, do not complicate the finding of the fast states and ensure the comparability of the dimensionless perturbation parameters. Moreover, a comparison is given between a model obtained by the usual approach of neglecting transmission lines with a model found by the approach taken here.

The paper is organized as follows: First, the model of the microgrid is introduced using the modeling procedure presented in [10]. Subsequently, the obtained full order model is normalized and the state variables are separated, according to the time scale they are associated to. Depending on this choice, multiple reduced order models are introduced. The models are evaluated by comparing simulation results. A conclusion is given at the end.

System Model

The considered configuration of the grid is depicted in Fig. 1. It can be operated in two modes. In grid-connected mode, there exists a connection to a stiff main grid and the two inverters support the grid. In islanded mode, this connection is cut and the grid is formed by the two inverters. In the following, the system model is introduced step-by-step for the inverters, the transmission lines, the load and the connection to the main grid. For the subsequent steps of model reduction, it is important that the variables are denoted in a common coordinate system. Here, a rotating coordinate system is used and three-phase quantities x_k, $k = 1, 2, 3$ are represented as complex variables as

$$\underline{x} = \tfrac{2}{3}\mathrm{e}^{-\mathrm{j}\theta}\left(1 \quad -\tfrac{1}{2}+\mathrm{j}\tfrac{\sqrt{3}}{2} \quad -\tfrac{1}{2}-\mathrm{j}\tfrac{\sqrt{3}}{2}\right)\begin{pmatrix}x_1 & x_2 & x_3\end{pmatrix}^{\mathrm{T}} \tag{1}$$

where θ is the grid angle of the first inverter modeled by

$$\dot{\theta} = \omega_1. \tag{2}$$

The first converter is taken as a reference because the mains with its fixed grid frequency is only available in grid-connected mode, see also [10] and [1].

In a later step, singular perturbation methods are applied for model reduction. In general, this is possible if certain parameters are much larger than others which allows then to split the system behavior into a 'fast' and a 'slow' one. For such a comparison, it is necessary to normalize the model which leads to dimensionless variables. This ensures that the magnitudes of the state variables—which may differ greatly—do not complicate the identification of the 'fast' variables. Consequently, all state variables x_i are normalized to their maximum expectable value $\hat{X}_i$ with $i = 1, 2, \ldots, n$ where n denotes the order of the system. The corresponding normalized state variable is then given by $\tilde{x}_i = x_i/\hat{X}_i$. For that, the apparent power delivered by an inverter is normalized to its nominal power $\hat{S} = 625\,\mathrm{kVA}$, and all voltages contained in the state equations are normalized to $\hat{V} = 490\,\mathrm{V}$ which is the phase to ground amplitude of the nominal grid voltage. Consequently, all currents of an inverter model according to Fig 2 are normalized to $\hat{I} = 3\hat{S}/(2\hat{V})$, whereas all currents that are to be assigned to the lines, the load or the main grid according to Fig. 1 are normalized to $2\hat{I}$. This is justified by the fact that the microgrid is fed by two inverters. With this, the parameter $\hat{R} = \hat{U}/\hat{I}$ denotes a resistance. Furthermore, each angular frequency is normalized to
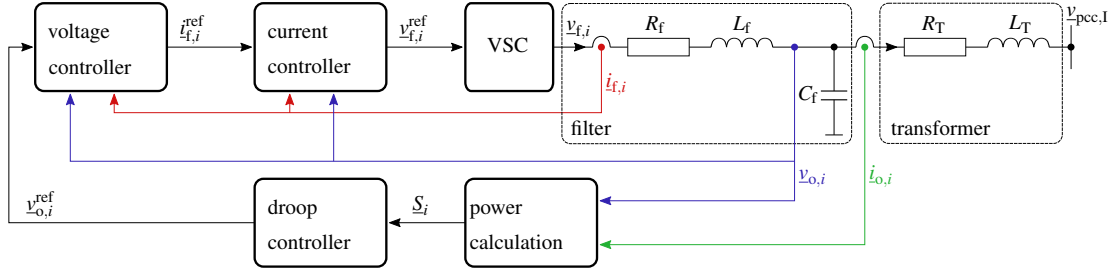
Fig. 2: Configuration of the grid-forming inverter $i = 1, 2$.

the nominal grid frequency ω_{nom}. The time t is normalized to a large time constant given by the cut-off frequency ω_c of the droop controller which will be introduced later. Hence, the relation of the time scales is captured by $\tilde{t} = \omega_c t$. For reasons of compactness, these preparatory steps are already included in the modeling which proceeds next. Note that the parameters on the left-hand-side of the following system equations, renamed as ε with an appropriate index, prepare the model for the model reduction procedure.

Inverter Model

The control scheme and schematic associated with the i-th, $i \in \{1, 2\}$, inverter is depicted in Fig. 2. It is adapted from [10] and is also used in [1]. A superordinated droop controller captures the power fed into the network. Based on this information, the droop controller determines the reference values for the frequency and the amplitude of the voltage $\underline{v}_{\text{o},i}$. In order to obtain the reference value $\underline{v}_{\text{f},i}^{\text{ref}}$ for the voltage outputted by the voltage source converter (VSC), each inverter is equipped with a voltage controller and a subordinated current controller. The output voltage of the VSC is filtered by an LC-Filter, where its output voltage $\underline{v}_{\text{o},i}$ is adapted to the voltage level of the transmission network by a transformer.

Using the common coordinates defined by the first inverter, the dynamics of the i-th inverter are modelled by

$$\frac{\mathrm{d}\underline{\tilde{S}}_i}{\mathrm{d}\tilde{t}} = \varepsilon_S \frac{\mathrm{d}\underline{\tilde{S}}_i}{\mathrm{d}\tilde{t}} = -\underline{\tilde{S}}_i + \underline{\tilde{v}}_{\text{o},i} \underline{\tilde{i}}_{\text{o},i}^* \tag{3a}$$

$$\frac{\omega_c}{\pi n_P \hat{S}} \frac{\mathrm{d}\delta_i}{\mathrm{d}\tilde{t}} = \varepsilon_\delta \frac{\mathrm{d}\delta_i}{\mathrm{d}\tilde{t}} = \mathrm{Re}\left(\underline{\tilde{S}}_1\right) - \mathrm{Re}\left(\underline{\tilde{S}}_i\right) \tag{3b}$$

$$\tilde{\omega}_i = 1 - \frac{2\pi n_P \hat{S}}{\omega_{\text{nom}}} \mathrm{Re}\left(\underline{\tilde{S}}_i\right) \tag{3c}$$

$$\underline{\tilde{v}}_{\text{o},i}^{\text{ref}} = \left(1 - \frac{n_Q \hat{S}}{\hat{V}} \mathrm{Im}\left(\underline{\tilde{S}}_i\right)\right) e^{j\delta_i} \tag{3d}$$

$$\frac{\omega_c}{\omega_{\text{nom}}} \frac{\mathrm{d}\underline{\tilde{\gamma}}_{1,i}}{\mathrm{d}\tilde{t}} = \varepsilon_{\gamma_1} \frac{\mathrm{d}\underline{\tilde{\gamma}}_{1,i}}{\mathrm{d}\tilde{t}} = -\left(\frac{2\omega_{\text{cf}}}{\omega_{\text{nom}}} + j\tilde{\omega}_1\right) \underline{\tilde{\gamma}}_{1,i} - \tilde{\omega}_i^2 \underline{\tilde{\gamma}}_{2,i} + \frac{2k_1 \hat{V} \omega_{\text{cf}}}{\hat{\Gamma}_1 \omega_{\text{nom}}} \left(\underline{\tilde{v}}_{\text{o},i}^{\text{ref}} - \underline{\tilde{v}}_{\text{o},i}\right) \tag{3e}$$

$$\frac{\omega_c}{\omega_{\text{nom}}} \frac{\mathrm{d}\underline{\tilde{\gamma}}_{2,i}}{\mathrm{d}\tilde{t}} = \varepsilon_{\gamma_2} \frac{\mathrm{d}\underline{\tilde{\gamma}}_{2,i}}{\mathrm{d}\tilde{t}} = \underline{\tilde{\gamma}}_{1,i} - j\tilde{\omega}_1 \underline{\tilde{\gamma}}_{2,i} \tag{3f}$$

$$\underline{\tilde{i}}_{\text{f},i}^{\text{ref}} = k_{\text{p,v}} \hat{R} \left(\underline{\tilde{v}}_{\text{o},i}^{\text{ref}} - \underline{\tilde{v}}_{\text{o},i}\right) + \frac{\hat{\Gamma}_1}{\hat{I}} \left(1 + \tilde{\omega}_i^2 L_f C_f\right) \underline{\tilde{\gamma}}_{1,i} - \underline{\tilde{i}}_{\text{f},i} \tag{3g}$$

$$\underline{\tilde{v}}_{\text{f},i}^{\text{ref}} = \underline{\tilde{v}}_{\text{f},i} = \frac{k_{\text{p,i}}}{\hat{R}} \left(\underline{\tilde{i}}_{\text{f},i}^{\text{ref}} - \underline{\tilde{i}}_{\text{f},i}\right) + \underline{\tilde{v}}_{\text{o},i} \tag{3h}$$

$$\omega_c \frac{L_f}{\hat{R}} \frac{\mathrm{d}\underline{\tilde{i}}_{\text{f},i}}{\mathrm{d}\tilde{t}} = \varepsilon_{i_f} \frac{\mathrm{d}\underline{\tilde{i}}_{\text{f},i}}{\mathrm{d}\tilde{t}} = \underline{\tilde{v}}_{\text{f},i} - \underline{\tilde{v}}_{\text{o},i} - \frac{1}{\hat{R}} \left(R_f + jL_f \omega_{\text{nom}} \tilde{\omega}_1\right) \underline{\tilde{i}}_{\text{f},i} \tag{3i}$$

$$\omega_c C_f \hat{R} \frac{\mathrm{d}\underline{\tilde{v}}_{\text{o},i}}{\mathrm{d}\tilde{t}} = \varepsilon_{v_o} \frac{\mathrm{d}\underline{\tilde{v}}_{\text{o},i}}{\mathrm{d}\tilde{t}} = \underline{\tilde{i}}_{\text{f},i} - \underline{\tilde{i}}_{\text{o},i} - j\hat{R} C_f \omega_{\text{nom}} \tilde{\omega}_1 \underline{\tilde{v}}_{\text{o},i} \tag{3j}$$

$$\omega_c \frac{L_T}{\hat{R}} \frac{\mathrm{d}\underline{\tilde{i}}_{\text{o},i}}{\mathrm{d}\tilde{t}} = \varepsilon_{i_o} \frac{\mathrm{d}\underline{\tilde{i}}_{\text{o},i}}{\mathrm{d}\tilde{t}} = \underline{\tilde{v}}_{\text{o},i} - \underline{\tilde{v}}_{\text{pcc,I}} - \frac{1}{\hat{R}} \left(R_T + jL_T \omega_{\text{nom}} \tilde{\omega}_1\right) \underline{\tilde{i}}_{\text{o},i} \tag{3k}$$

The submodel (3) can be subdivided as follows:

- Equations (3a)-(3d) and constitute the droop controller. The apparent power is filtered by a first order low-pass filter with the cut-off frequency ω_c which yields $\underline{\tilde{S}}_i$. With this information, the reference values $\tilde{\omega}_i$ and $\underline{\tilde{v}}_{o,i}^{\mathrm{ref}}$ for the output voltage and the frequency, respectively, are determined. These references are governed by the frequency-active power droop law (3c) and the voltage-reactive power droop law (3d), where n_P and n_Q are the droop parameters [10]. Since the voltage-reactive power droop law according to [10] defines only the magnitude but not the phase angle of the reference voltage $\underline{\tilde{v}}_{o,i}^{\mathrm{ref}}$, the difference angle δ_i must be taken into account, when referring to the common coordinate system. This angle, whose derivative is given by (3b) represents the load distribution among the i-th and the first inverter and results from the active power droop control of the individual inverters that causes different inverter frequencies $\tilde{\omega}_i$ [10]. Since the angle δ_i is dimensionless and expected to vary within a interval $[-\pi/2, \pi/2]$, the angle is not normalized. According to (3b), $\delta_1 = 0$ applies at all times.
- The cascaded voltage controller with inner current loop is constituted by (3e)-(3h). According to (3e)-(3g), the voltage controller, whose dynamics are captured by (3e) and (3f), is implemented as so-called proportional resonant controller with the proportional gain $k_{p,v}$, the resonant gain k_I and the frequency ω_{cf}. The reference current $\underline{i}_{f,i}^{\mathrm{ref}}$ is propagated to the subordinated current controller (3h) with gain $k_{p,i}$. In order to obtain dimensionless state variables that represent the voltage controller, the states $\tilde{\underline{\gamma}}_{1,i}$ and $\tilde{\underline{\gamma}}_{2,i}$ are normalized to $\hat{\Gamma}_1 = 2\hat{I}/(1+\omega_{\mathrm{nom}}^2 L_f C_f)$ and $\hat{\Gamma}_2 = \hat{\Gamma}_1/\omega_{\mathrm{nom}}$, respectively. Note that the operation of the VSC is assumed to be ideal, hence $\underline{v}_{f,i}^{\mathrm{ref}} = \underline{v}_{f,i}$ applies.
- Equations (3i) and (3j) describe the dynamics of the LC-filter. The filter features an inductance L_f and a capacitance C_f, respectively. Furthermore, the filter is damped by a resistance R_f.
- The grid connecting transformer is modeled according to (3k) by its short circuit inductance L_T and resistance R_T.

Load Model

The load is considered to be a passive RL-load. In the common reference frame it can be modeled as

$$2\omega_c \frac{L_L}{\hat{R}} \frac{d\underline{\tilde{i}}_L}{d\tilde{t}} = \varepsilon_{i_L} \frac{d\underline{\tilde{i}}_L}{d\tilde{t}} = \underline{\tilde{v}}_{\mathrm{pcc,L}} - \frac{2}{\hat{R}}\left(R_L + j\omega_{\mathrm{nom}}L_L\tilde{\omega}_1\right)\underline{\tilde{i}}_L \tag{4}$$

where $\underline{v}_{\mathrm{pcc,L}}$ is the voltage of the network node that is connected to the load and R_L and L_L are the parameters of the load.

Model of the Connection to the Main Grid

The local grid is optionally connected to a main grid by a transformer. Considering the grid frequency as ω_{nom} and its voltage amplitude as v_{nom}, the connecting transformer can be modelled as

$$\frac{\omega_c}{\pi n_P \hat{S}} \frac{d\delta_g}{d\tilde{t}} = \varepsilon_\delta \frac{d\delta_g}{d\tilde{t}} = \underline{\tilde{S}}_1 + \underline{\tilde{S}}_1^* \tag{5a}$$

$$2\omega_c \frac{L_g}{\hat{R}} \frac{d\underline{\tilde{i}}_g}{d\tilde{t}} = \varepsilon_{i_g} \frac{d\underline{\tilde{i}}_g}{d\tilde{t}} = e^{j\delta_g} - \underline{\tilde{v}}_{\mathrm{pcc,G}} - \frac{2}{\hat{R}}\left(R_g + j\omega_{\mathrm{nom}}\tilde{\omega}_1 L_g\right)\underline{\tilde{i}}_g \tag{5b}$$

with its parameters R_g and L_g. Due to the droop control, the frequency of the the grid-forming inverters may differ from the the main grid frequency ω_{nom}. This is why, a difference angle δ_g between the main grid voltage and the voltage of the first inverter must be considered. As shown in (5b), this angle has to be taken into account when referring to the common reference frame.

Network Model

According to Fig. 1, the dynamics of the network are captured by

$$\frac{1}{2}\omega_c \hat{R} C_{2k} \frac{d\underline{\tilde{v}}_{\mathrm{pcc,I}}}{d\tilde{t}} = \varepsilon_{v_{\mathrm{pcc,L}}} \frac{d\underline{\tilde{v}}_{\mathrm{pcc,I}}}{d\tilde{t}} = \frac{1}{2}\left(\underline{\tilde{i}}_{o,1} + \underline{\tilde{i}}_{o,2}\right) - \underline{\tilde{i}}_{2k} - \frac{j}{2}\omega_{\mathrm{nom}}\hat{R}C_{2k}\tilde{\omega}_1\underline{\tilde{v}}_{\mathrm{pcc,I}} \tag{6a}$$

$$2\omega_c \frac{L_{2k}}{\hat{R}} \frac{d\underline{\tilde{i}}_{2k}}{d\tilde{t}} = \varepsilon_{i_{2k}} \frac{d\underline{\tilde{i}}_{2k}}{d\tilde{t}} = \underline{\tilde{v}}_{\mathrm{pcc,I}} - \underline{\tilde{v}}_{\mathrm{pcc,L}} - \frac{2}{\hat{R}}\left(R_{2k} + j\omega_{\mathrm{nom}}L_{2k}\tilde{\omega}_1\right)\underline{\tilde{i}}_{2k} \tag{6b}$$

$$\frac{1}{2}\omega_\mathrm{c}\hat{R}\left(C_\mathrm{2k}+C_\mathrm{16k}\right)\frac{\mathrm{d}\tilde{v}_\mathrm{pcc,L}}{\mathrm{d}\tilde{t}}=\varepsilon_{v_\mathrm{pcc,L}}\frac{\mathrm{d}\tilde{v}_\mathrm{pcc,L}}{\mathrm{d}\tilde{t}}=\tilde{\underline{i}}_\mathrm{2k}+\tilde{\underline{i}}_\mathrm{16k}-\tilde{\underline{i}}_\mathrm{L}-\frac{\mathrm{j}}{2}\omega_\mathrm{nom}\hat{R}\left(C_\mathrm{2k}+C_\mathrm{16k}\right)\tilde{\omega}_1\tilde{v}_\mathrm{pcc,L} \tag{6c}$$

$$2\omega_\mathrm{c}\frac{L_\mathrm{16k}}{\hat{R}}\frac{\mathrm{d}\tilde{\underline{i}}_\mathrm{16k}}{\mathrm{d}\tilde{t}}=\varepsilon_{i_\mathrm{16k}}\frac{\mathrm{d}\tilde{\underline{i}}_\mathrm{16k}}{\mathrm{d}\tilde{t}}=\tilde{\underline{v}}_\mathrm{pcc,G}-\tilde{\underline{v}}_\mathrm{pcc,L}-\frac{2}{\hat{R}}\left(R_\mathrm{16k}+\mathrm{j}\omega_\mathrm{nom}L_\mathrm{16k}\tilde{\omega}_1\right)\tilde{\underline{i}}_\mathrm{16k} \tag{6d}$$

$$\frac{1}{2}\omega_\mathrm{c}\hat{R}C_\mathrm{16k}\frac{\mathrm{d}\tilde{v}_\mathrm{pcc,G}}{\mathrm{d}\tilde{t}}=\varepsilon_{v_\mathrm{pcc,G}}\frac{\mathrm{d}\tilde{v}_\mathrm{pcc,G}}{\mathrm{d}\tilde{t}}=\tilde{\underline{i}}_\mathrm{g}-\tilde{\underline{i}}_\mathrm{16k}-\frac{\mathrm{j}}{2}\omega_\mathrm{nom}\hat{R}C_\mathrm{16k}\tilde{\omega}_1\tilde{v}_\mathrm{pcc,G}. \tag{6e}$$

where all quantities are denoted in the common coordinate system defined by the first inverter.

Model Reduction

Singular Perturbation Theory

The full-order model (3)-(6) is considered here to describe the behavior of the system in the most detailed way. From practical experience, it is well known that some of its variables change 'slowly' in time while others change 'fast'. For some applications, the 'fast' behavior is outside the focus of investigation. Furthermore, due to the quite high number $n = 41$ of states, a simulation might be computationally expensive. This motivates to work with reduced models instead that approximate the behavior of the full-order model. Such a model reduction can be obtained by applying singular perturbation theory. This has been done for electrical machines [11], power electronic converters [12, 13], and also for island grids [1–4].

An introduction to singular perturbation theory can be found in [6, 8, 9]. According to these references, the standard form for singular perturbation model reduction reads

$$\dot{\boldsymbol{x}}=\boldsymbol{f}(t,\boldsymbol{x},\boldsymbol{z},\varepsilon) \tag{7a}$$
$$\varepsilon\dot{\boldsymbol{z}}=\boldsymbol{g}(t,\boldsymbol{x},\boldsymbol{z},\varepsilon). \tag{7b}$$

with the 'fast states' $\boldsymbol{z}=(z_1,\ldots,z_m)^\mathrm{T}$, the 'slow states' $\boldsymbol{x}=(x_1,\ldots,x_{n-m})^\mathrm{T}$, and the perturbation parameter ε. The subsystem (7b) is referred to as boundary-layer system. Setting the perturbation parameter ε to zero and solving

$$0=\boldsymbol{g}(t,\boldsymbol{x},\boldsymbol{z},0) \tag{8}$$

for $\boldsymbol{z}$ yields the quasi steady state solution $\boldsymbol{z}^\mathrm{qss}=\boldsymbol{\phi}(t,\boldsymbol{x})$ for the fast states. The reduced model is then given by

$$\dot{\boldsymbol{x}}=\boldsymbol{f}(t,\boldsymbol{x},\boldsymbol{\phi}). \tag{9}$$

To find out whether the fast variables $\boldsymbol{z}$ converge to their steady state solution $\boldsymbol{z}^\mathrm{qss}$, a stability condition must be satisfied that guarantees that $\boldsymbol{z}$ will remain close to its equilibrium $\boldsymbol{z}^\mathrm{qss}$, while the slow states $\boldsymbol{x}$ are slowly varying [6, 8, 9]. This stability property is met if the equilibrium $\boldsymbol{z}^\mathrm{qss}$ of the boundary-layer system (7b) is exponentially stable. According to [6, 8, 9], the stability property is satisfied if the Jacobian $\partial\boldsymbol{g}/\partial\boldsymbol{z}$ at $\varepsilon=0$ is nonsingular for all $(\boldsymbol{x},\boldsymbol{z})\in D$ and the real parts of its eigenvalues are negative for all $(\boldsymbol{x},\boldsymbol{z})\in D$, where D is a region of interest for the present analysis. Hence, the stability property can be expressed as

$$\det\left(\frac{\partial\boldsymbol{g}}{\partial\boldsymbol{z}}\right)\bigg|_{\varepsilon=0}\neq 0,\qquad \forall(\boldsymbol{x},\boldsymbol{z})\in D \tag{10a}$$

$$\mathrm{Re}\left[\lambda\left\{\frac{\partial\boldsymbol{g}}{\partial\boldsymbol{z}}\right\}\right]\bigg|_{\varepsilon=0}<-c<0,\qquad \forall(\boldsymbol{x},\boldsymbol{z})\in D, \tag{10b}$$

in which $\lambda\{\partial\boldsymbol{g}/\partial\boldsymbol{z}\}$ is an eigenvalue of the Jacobian matrix, and c is a fixed positive number.

The full-order model (3)-(6) can be brought into the standard form (7) by applying the following procedure: In a preparatory step, the model (3)-(6) is rewritten in a rearranged order as

$$\boldsymbol{\varepsilon}\circ\dot{\boldsymbol{\zeta}}=\boldsymbol{\psi}(t,\boldsymbol{\zeta},\boldsymbol{\varepsilon}), \tag{11}$$
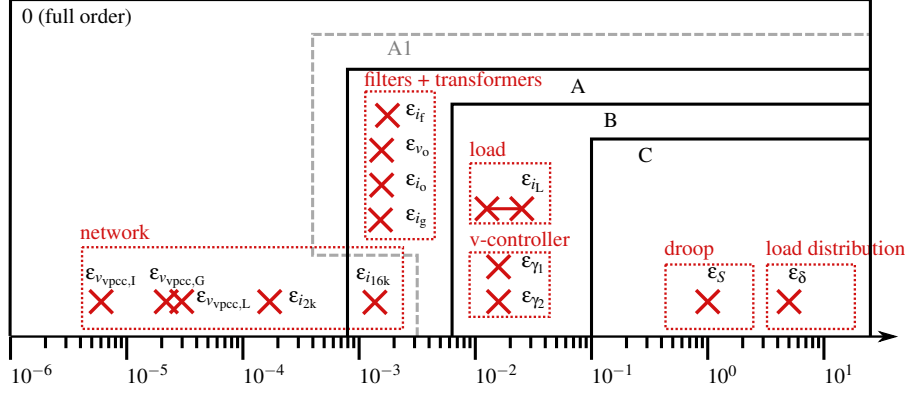
Fig. 3: Comparison of perturbation parameters

with the state vector $\boldsymbol{\zeta} = (\zeta_1, \ldots, \zeta_n)^{\mathrm{T}}$, $\zeta_i \in \{\tilde{\delta}_1, \ldots, \tilde{\underline{v}}_{\mathrm{pcc,G}}\}$ and the corresponding perturbation parameters $\boldsymbol{\varepsilon} = (\varepsilon_1, \ldots, \varepsilon_n)^{\mathrm{T}}$ with $\varepsilon_i \in \{\varepsilon_\delta, \ldots, \varepsilon_{v_{\mathrm{pcc,G}}}\}$. The vector $\boldsymbol{\psi} = (\psi_1, \ldots, \psi_n)^{\mathrm{T}}$ of functions contains the corresponding functions on the right-hand-side. The rearrangement is done such that $\varepsilon_{i+1} \leq \varepsilon_i$. Next, choose $\varepsilon \in (\varepsilon_n, \varepsilon_1)$ in a way that the parameters ε_i are split in two non-empty groups: the group with $\varepsilon_i \leq \varepsilon$ and the group $\varepsilon_i > \varepsilon$. Rewrite the lines of (11) as

$$\dot{\zeta}_i = \frac{1}{\varepsilon_i} \psi_i(t, \boldsymbol{\zeta}, \boldsymbol{\varepsilon}) \quad \text{for } \varepsilon_i > \varepsilon, i = 1, 2, \ldots, n-m \tag{12}$$

$$\varepsilon \dot{\zeta}_i = \frac{\varepsilon}{\varepsilon_i} \psi_i(t, \boldsymbol{\zeta}, \boldsymbol{\varepsilon}) \quad \text{for } \varepsilon_i \leq \varepsilon, i = n-m+1, n-m+2, \ldots, n. \tag{13}$$

By subsequently setting

$$\boldsymbol{x} = (\zeta_1, \ldots, \zeta_{n-m})^{\mathrm{T}}$$
$$\boldsymbol{z} = (\zeta_{n-m+1}, \ldots, \zeta_n)^{\mathrm{T}}$$
$$\boldsymbol{f}(t, \boldsymbol{x}, \boldsymbol{z}, \boldsymbol{\varepsilon}) = \left(\frac{1}{\varepsilon_1} \psi_1(t, \boldsymbol{\zeta}, \boldsymbol{\varepsilon}), \ldots, \frac{1}{\varepsilon_{n-m}} \psi_{n-m}(t, \boldsymbol{\zeta}, \boldsymbol{\varepsilon}) \right)^{\mathrm{T}}$$
$$\boldsymbol{g}(t, \boldsymbol{x}, \boldsymbol{z}, \boldsymbol{\varepsilon}) = \left(\frac{\varepsilon}{\varepsilon_{n-m+1}} \psi_{n-m+1}(t, \boldsymbol{\zeta}, \boldsymbol{\varepsilon}), \ldots, \frac{\varepsilon}{\varepsilon_n} \psi_n(t, \boldsymbol{\zeta}, \boldsymbol{\varepsilon}) \right)^{\mathrm{T}},$$

the model is obtained in the standard form (7).

Reduced-Order Models

The values of the elements of $\boldsymbol{\varepsilon}$, i.e. the perturbation parameters, are shown in Fig. 3. It is possible to identify groups by value and by topic and it is interesting to see that these two kinds of grouping may lead to different results. The basic idea is now to derive models of reduced order in a stepwise fashion. Therefore, according to a grouping scheme, some equations are considered to constitute the fast subsystem. Grouping by value is equivalent to choosing ε in order to obtain the form (12), (13). The quasi steady-state solution of the fast subsystem is substituted into the slow subsystem, see (8) and (9). This gives a reduced order model. The same procedure can be repeated and leads to models with an even lower order of the system.

For the particular system investigated here, this process is shown in Fig. 4. Since it is common practice to group by topic and to neglect the dynamics of the connecting network [1], Model A1 is derived from Model 0. However, grouping by value leads to Model A, where the dynamics of the long transmission line is associated with the slow subsystem because $\varepsilon_{i_{16k}}$ is much larger than the other parameters associated with the network. Models B and C are subsequently derived from Model A. As a result, a series of models of decreasing order is obtained.
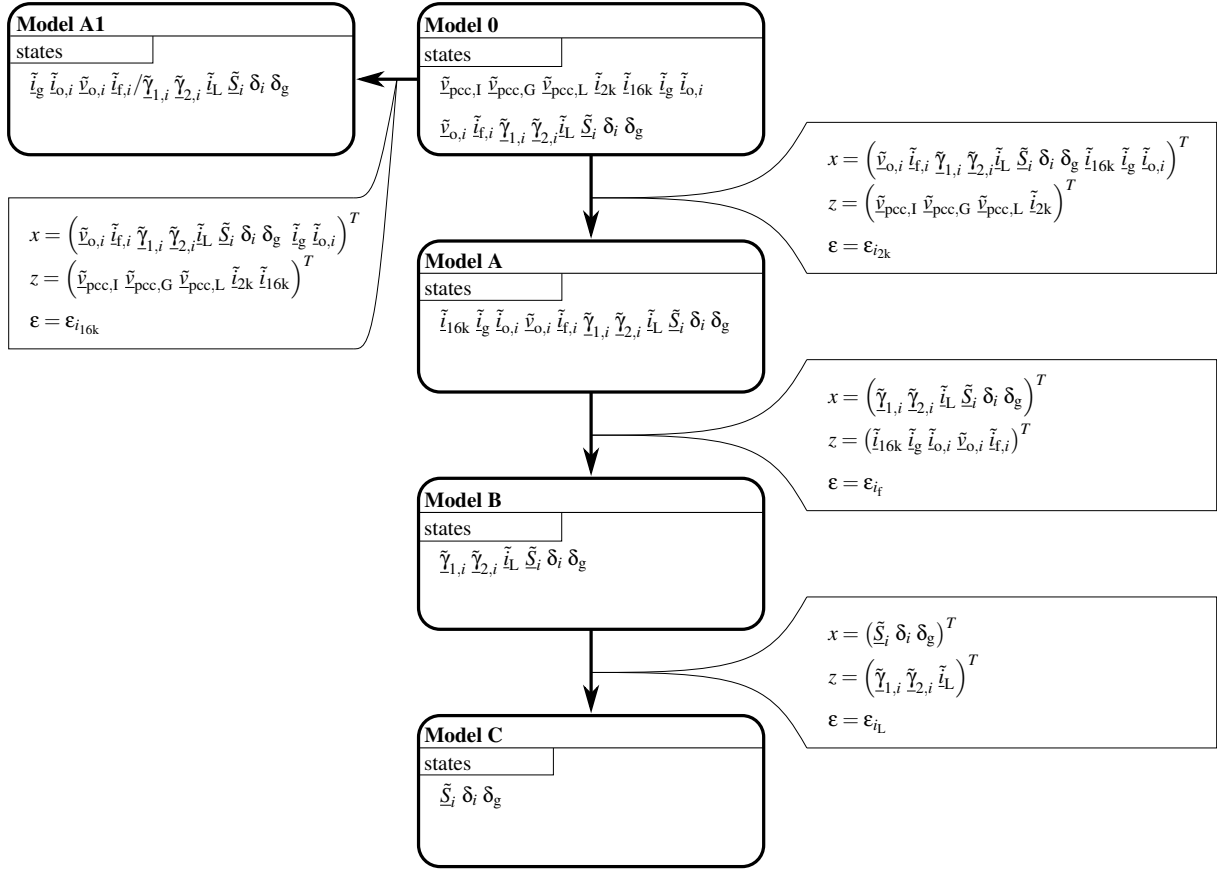
Fig. 4: Successive model reduction procedure

Numerical Case Studies

The effect on the modeling accuracy due to model reduction is investigated by comparing simulation results of the reduced-order models with the full-order model. The parameters of the system are provided by Table I. The system behavior under the influence of a sudden load step is considered. In a first series of experiments, the system is simulated in islanded mode. The corresponding results are depicted in Figs. 5 and 6. In a second experiment, the heuristic approach of model reduction leading to Model A1 is compared to Model A. For this purpose, the sytem operates in grid connected mode and the results are given in Fig. 7. From these results, the following conclusions can be drawn:

- Model A is particularly suitable for examining effects evolving in the interval $t \in [0, 0.02\,\text{s}]$ which are caused by the dynamics of the filter and the transformers. Resonance effects as a result of the network dynamics are not captured by Model A.

Table I: Parameters of the system

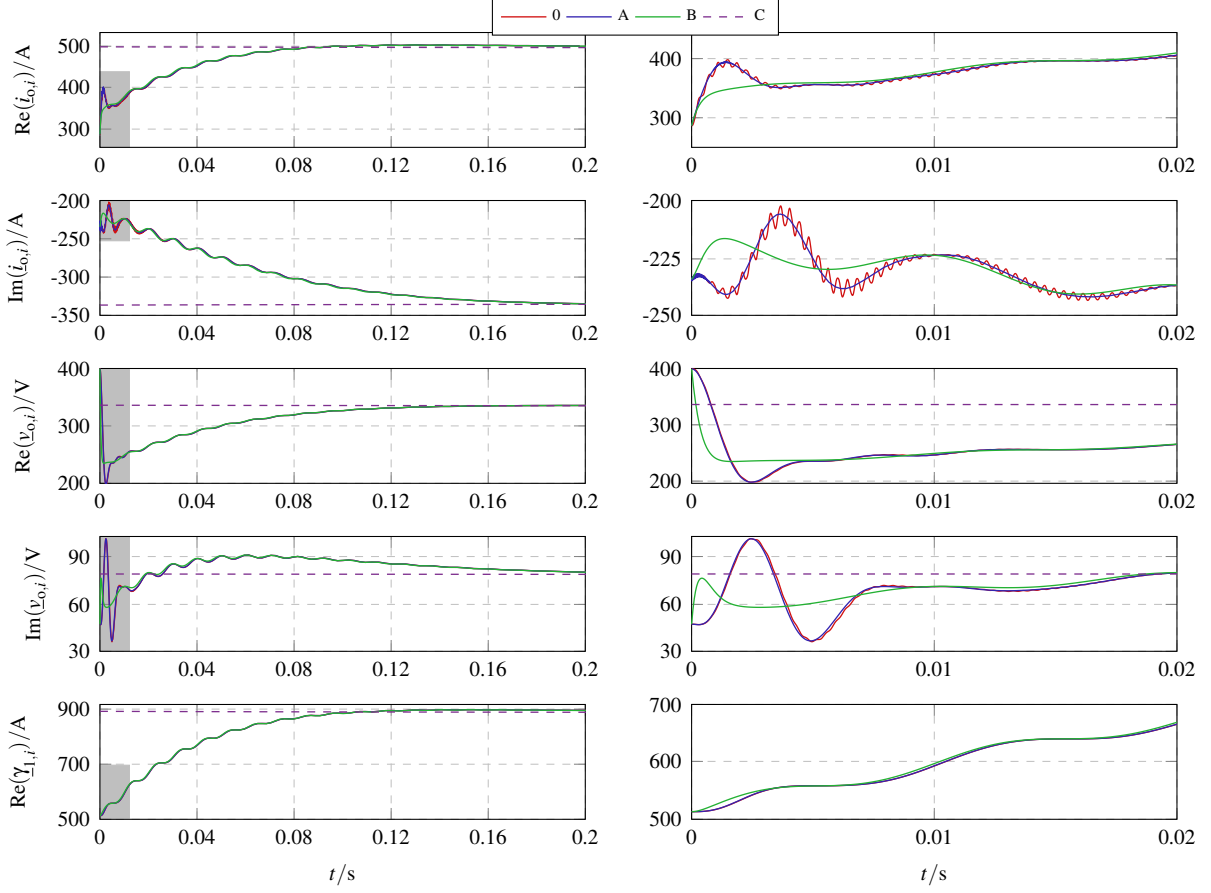| component	values
filter	$L_\text{f} = 200\,\mu\text{H}, C_\text{f} = 540\,\mu\text{F}, R_\text{f} = 2\,\text{m}\Omega$
inverter transformer	$L_\text{T} = 177\,\mu\text{H}, R_\text{T} = 15.4\,\text{m}\Omega$
2 km-line	$L_\text{2k} = 9.6\,\mu\text{H}, C_\text{2k} = 4.17\,\mu\text{F}, R_\text{2k} = 5.8\,\text{m}\Omega$
16 km-line	$L_\text{16k} = 77\,\mu\text{H}, C_\text{16k} = 16.7\,\mu\text{F}, R_\text{16k} = 23\,\text{m}\Omega$
mains transformer	$L_\text{g} = 89.5\,\mu\text{H}, R_\text{g} = 6.2\,\text{m}\Omega$
nominal voltage and frequency	$v_\text{nom} = \frac{\sqrt{2}}{\sqrt{3}}600\,\text{V}, f_\text{nom} = 50\,\text{Hz}$
droop controller	$n_\text{P} = 0.5\,\mu\text{Hz}\,\text{W}^{-1}, n_\text{Q} = 33.3\,\mu\text{Vvar}^{-1}, \omega_\text{c} = 5\,\text{s}^{-1}$
voltage and current controller	$k_\text{p,v} = 0.6\,\text{S}, k_\text{I} = 6\,\text{S}, \omega_\text{cf} = 10\,\text{s}^{-1}, k_\text{p,i} = 0.9\,\Omega$

Fig. 5: Simulation results in islanded mode. A load step at $t = 0$ is considered. The results are plotted on a long time scale (left) and on a short time scale (right). The output current $i_{o,i}$ of the i-th inverter, the voltage $\underline{v}_{o,i}$ across the filter capacitor of the i-th inverter, and a state $\underline{\gamma}_{1,i}$ associated with the voltage controller of the i-th inverter are displayed

- Model B delivers sufficiently accurate results for investigating processes that take place in the interval $t \in [0, 0.2\,\text{s}]$. Therefore, Model B is suitable to examine effects due to the voltage controller dynamics.
- As shown in Fig. 6, when considering processes taking place in $t \in [0, 0.2\,\text{s}]$, Model C yields poor results. Therefore, Model C is not suitable for investigating effects caused by the low-pass filters of the droop controller. However, Model C can be used for long time simulations of the microgrid, where the power sharing among the inverters is of interest.
- As shown in Fig. 7, Model A delivers significantly better results compared to Model A1. This is observed even though Model A1 has only one complex state less than Model A. This highlights the importance of the separation according to the corresponding perturbation parameters. Thus, it can
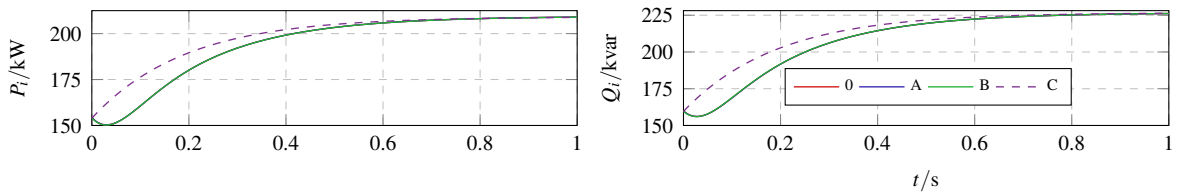

Fig. 6: Simulation results in islanded mode. A load step at $t = 0$ is considered. The low-pass filtered active and reactive Power P_i and Q_i delivered by the i-th inverter are displayed.
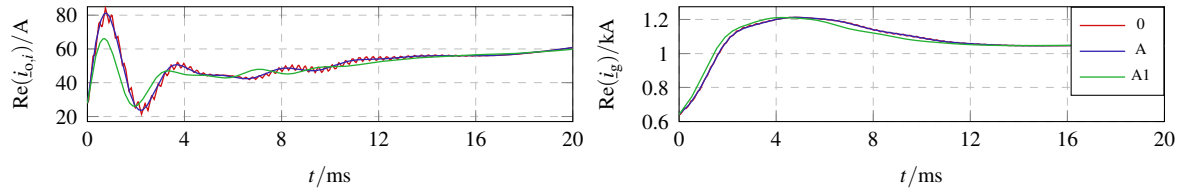
Fig. 7: The system is simulated in grid-connected mode. A load step at $t = 0$ is considered. The simulation results for the full order Model 0, the reduced Model A, and the reduced Model A1, where the dynamic network model has been replaced by an algebraic model are compared. The real values of the i-th inverter output current $\underline{i}_{o,i}$ and the current $\underline{i}_g$ delivered by the main grid are displayed.

Table II: Comparison of the models in terms of computational effort

	number of states	solver steps
Model 0	41	3489
Model A	33	360
Model A1	31	353
Model B	17	336
Model C	7	57

be concluded that the heuristic approach of neglecting the dynamic behavior of the transmission network, which is common in the modeling of network applications [1], can lead to inaccurate results. The models are compared in terms of computational effort by investigating the number of solver steps. The obtained results are shown in Table II for a time horizon of $t = 2\,\mathrm{s}$ using a stiff solver (ode23tb).

Conclusion

Singular perturbation methods were successfully applied for model reduction in a microgrid application. The method proposed here allows to separate the full-order dynamics into a fast and a slow subsystem. The splitting can be done according to the respective modeling purpose. As a result, multiple reduced models of descending order were obtained that reduce the computational effort for simulations. The method does not require calculation of eigenvalues nor empirical knowledge of the system. Moreover, it was shown that the heuristic approach of neglecting the dynamic behavior of the transmission network, which is common in the modeling of network applications, can lead to inaccurate results which can be avoided by using the method.

References

[1] L. Luo and S. V. Dhople. Spatiotemporal model reduction of inverter-based islanded microgrids. *IEEE Transactions on Energy Conversion*, 29(4):823–832, 2014.

[2] K. Kodra, Ningfan Z., and Z. Gajić. Model order reduction of an islanded microgrid using singular perturbations. In *2016 American Control Conference (ACC)*, pages 3650–3655, 2016.

[3] Y. Peng, et al. Reduced order modeling method of inverter-based microgrid for stability analysis. In *2017 IEEE Applied Power Electronics Conference and Exposition (APEC)*, pages 3470–3474, 2017.

[4] V. Mariani, F. Vasca, and J. M. Guerrero. Analysis of droop controlled parallel inverters in islanded microgrids. In *2014 IEEE International Energy Conference (ENERGYCON)*, pages 1304–1309, 2014.

[5] M. Rasheduzzaman, J. A. Mueller, and J. W. Kimball. Reduced-order small-signal model of microgrid systems. *IEEE Transactions on Sustainable Energy*, 6(4):1292–1305, 2015.

[6] P.V. Kokotovic, R.E. O'Malley, and P. Sannuti. Singular perturbations and order reduction in control theory — an overview. *Automatica*, 12(2):123–132, 1976.

[7] G. Peponides, P. Kokotovic, and J. Chow. Singular perturbations and time scales in nonlinear models of power systems. *IEEE Transactions on Circuits and Systems*, 29(11):758–767, 1982.

[8] H. K. Khalil. *Nonlinear Systems*. Pearson Education. Prentice Hall, 2002.

[9] P. Kokotovic, H. K. Khalil, and J. O'Reilly. *Singular Perturbation Methods in Control: Analysis and Design*. Classics in Applied Mathematics. Society for Industrial and Applied Mathematics (SIAM), 1999.

[10] N. Pogaku, M. Prodanovic, and T. C. Green. Modeling, analysis and testing of autonomous operation of an inverter-based microgrid. *IEEE Transactions on Power Electronics*, 22(2):613–625, 2007.

[11] Z. Sorchini and Ph. T. Krein. Formal derivation of direct torque control for induction machines. *IEEE Trans. Power Electron.*, 21(5):1428–1436, Sep. 2006.

[12] J. W. Kimball and Ph. T. Krein. Singular perturbation theory for DC-DC converters and application to PFC converters. *IEEE Trans. Power Electron.*, 23(6):2970–2981, Dec. 2008.

[13] A. Gensior and H. Fehr. Modeling and energy balancing control of modular multilevel converters using perturbation theory for quasi-periodic systems. *IEEE Trans. Power Electron.*, 36(2):2201–2217, 2021.